8-17-2020

Underground Wireless Channel Bandwidth and Capacity

Abdul Salam
Purdue University, salama@purdue.edu

Usman Raza
Purdue University

Chapter 5
Underground Wireless Channel Bandwidth and Capacity

Abstract The UG channel bandwidth and capacity are vital parameters in wireless underground communication system design. In this chapter, a comprehensive analysis of the wireless underground channel capacity is presented. The impact of soil on return loss, bandwidth and path loss are discussed. The results of underground multi-carrier modulation capacity are also outlined. Moreover, the single user capacity and multi-carrier capacity is also introduced with an in-depth treatment of soil texture, soil moisture, and distance e ects on channel capacity. Finally, the chapter is concluded with discussion of challenges and open research issues.

5.1 Introduction

The analysis of the capacity in wireless underground channel is challenging due to many factors: first, when an electromagnetic wave is incident into soil, the wavelength changes because of the higher permittivity of soil compared to that of air [61]. Soil permittivity depends on soil properties, such as bulk density, soil texture, soil moisture (Volumetric Water Content), salinity, and temperature. Second, when an antenna is buried underground, its return loss property changes due to the high permittivity of the soil [54]. Moreover, with the variation in soil moisture and hence soil permittivity, the return loss of the antenna varies too. Fig. 5.1 shows the organizational structure of the chapter. The wireless underground channel capacity is discussed next.

5.2 Wireless Underground Channel Capacity

The single and multi-user capacity of wireless underground channel is discussed in the following sections.

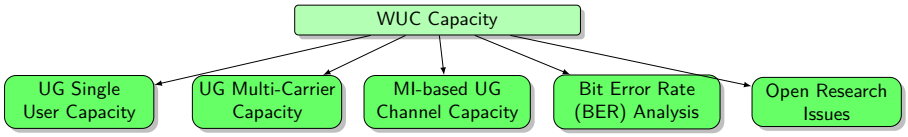

Fig. 5.1: Organization of the Chapter

5.3 Single User Capacity

The channel capacity, in a wireless communication, is calculated as :

$$C = B\log_2\left(1 + \frac{S}{N_0 B}\right), \tag{5.1}$$

where B denotes the system bandwidth, S denotes the received signal strength at receiver and N_0 denotes the noise power density. The analysis consider the maximum bandwidth for antenna design. Received signal strength of the signal is e ected by the antenna return loss and is given as:

$$S_{\mathrm{dB}} = P_t + 10log_{10}(1 - 10^{-\frac{RL_{\mathrm{dB}}}{10}}) - L, \tag{5.2}$$

where RL_{dB} antenna return loss, L is the path loss. The interference in wireless communication is not that big. It is because of less number of devices, hence, noise is mainly thermal noise and can be considered constant [26, 44].

5.3.1 Numerical Analysis

This section discusses the experiments conducted to understand the soil impact on underground wireless communication In coming sections, the discussion on how propagation loss, return loss and bandwidth of antenna are e ected by soil. Moreover, it also analyzes how channel capacity response to changing frequencies and soil moisture level. The default parameters for the experiments, unless a change is specified explicitly, are as follow: soil type is clay soil (having $31\,\%$ clay and $29\,\%$ sand), depth of underground device is 0.4m and that of above-ground is 2.5m, and length of antenna is $60\,\mathrm{mm}$ with diameter of 2mm.

To assess the performance of UG channel we have analyzed the UG channel capacity. Our analysis shows that higher soil moisture a ects the path loss and capacity of UG channel. Change in the path loss and capacity with soil moisture in silt loam testbed for $200\,\mathrm{MHz}$, $500\,\mathrm{MHz}$ and $700\,\mathrm{MHz}$ frequencies is shown in Fig. 5.2. We can see from Fig. 5.2 (a) that when soil moisture is decreased, there is $5\,\mathrm{dB}$ to $8\,\mathrm{dB}$ decrease in path loss at $200\,\mathrm{MHz}$ frequency, $25\,\mathrm{dB}$ decrease at $500\,\mathrm{MHz}$ and $15\,\mathrm{dB}$ decrease in path loss is observed at $700\,\mathrm{MHz}$ frequency. This is caused by

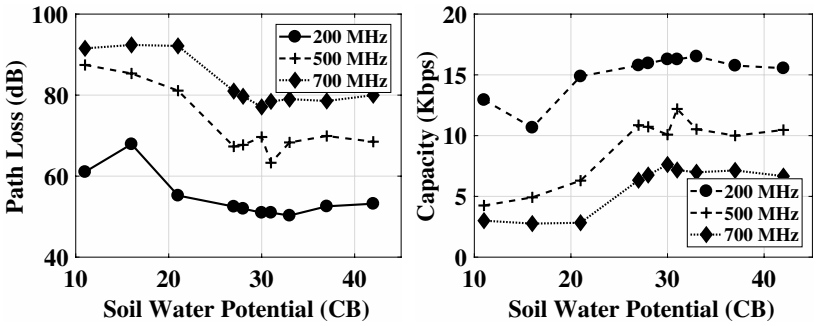

(a) (b)

Fig. 5.2: E ects of change in soil moisture on (a)) path Loss, (b)) channel capacity

higher permittivity of the soil at higher soil moisture, higher attenuation of waves causes higher path loss.

Similarly in Fig. 5.2(b) we can see that capacity is increased with decrease in soil moisture for all three frequencies. Due to the fact that in most situations, sandy soil has lower path loss, it has a higher capacity than the silt loam soil in most situations. Each soil has an optimal operation frequency region where the communication achieves the maximum capacity. However, unlike over-the-air communications, the optimal frequency where the maximum capacity is achieved is not the same as the resonant frequency of the antenna. Moreover, since changes in soil moisture a ects the path loss, return loss, and bandwidth of antenna, hence, capacity achieving frequency spectrum changes as well. This is because lateral wave and reflected wave [61] experience more attenuation as the burial depth of the antenna is increased. Therefore, in UG communications, the e ects of the antenna, and the soil need to be considered together to find the optimal operation frequency.

5.3.2 Soil Impact on Return Loss, Bandwidth and Path Loss

Fig. 5.3(a) shows the negative of return loss (S_{11}) at frequency range of $100\,\mathrm{MHz}$ to $1\,\mathrm{GHz}$. Volumetric Water Content (VWC) is the major way to indicate soil moisture and is calculated as a ratio of water in a soil-water mixture. It analyzes the e ect with VWC at $20\,\%$, $25\,\%$, $30\,\%$, $35\,\%$ and $40\,\%$. VWC inversely impacts the resonant frequency. Increasing the VWC values significantly decrease the resonant frequency, e.g., as shown, the frequency decreased approximately $33\,\%$, i.e., from $649\,\mathrm{MHz}$ to $432\,\mathrm{MHz}$, with a VWC increase of $20\,\%$ to $40\,\%$.

Fig. 5.3(b) plots the antenna bandwidth with operation frequency at changing soil moisture levels and return loss threshold δ of $-10\,\mathrm{dB}$. Bandwidth is given as a range of frequency where the return loss is less than the threshold. Therefore,

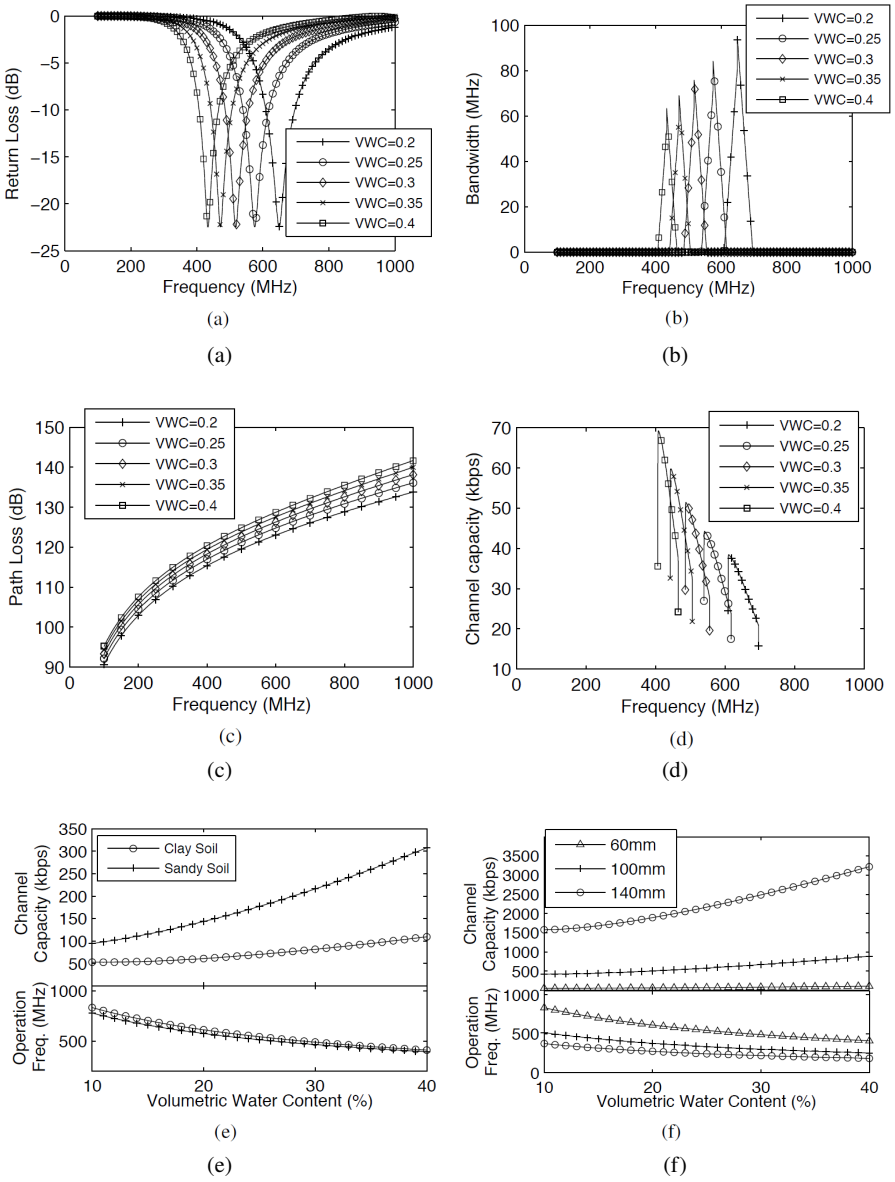

Fig. 5.3: Numerical results from experiments: (a) Return Loss, (b) Bandwidth, (c) Path loss in UG2AG channel, (d) Capacity in UG2AG link, (e) Capacity at di erent frequencies and soil moisture values, (f) Capacity at di erent frequencies and antenna sizes,[10]

system achieves the highest bandwidth at resonant frequency and its suddenly start decrease out of the resonant frequency. For example, for VWC = $40\,\%$ the bandwidth decreases approximately $16\,\%$, i.e., from $62\,\mathrm{MHz}$ (at resonant frequency of $434\,\mathrm{MHz}$) to $52\,\mathrm{MHz}$ (operational frequency of $433\,\mathrm{MHz}$). Similarly, the bandwidth is inversely e ected by VWC at a given resonant frequency. It can be observed that, at resonant frequency, the bandwidth is $94\,\mathrm{MHz}$ at $20\,\%$ VWC, and drops to $74\,\mathrm{MHz}$ and $62\,\mathrm{MHz}$ with a VWC increase of $20\,\%$ & $40\,\%$, respectively.

Fig. 5.3(c) shows the path loss for UG2AG channel, with frequency at changing soil moisture [29, 35]. It can be observed that path loss is directly proportional to VWC and frequency. Soil moisture a ect the path loss and this e ect is significantly higher at higher frequencies. For example, as shown in the Fig. 5.3(c), path loss is $107.6\,\mathrm{dB}$ for a VWC of $40\,\%$ and frequency of $200\,\mathrm{MHz}$. With same frequency, it changes $102.9\,\mathrm{dB}$ at VWC of $20\,\%$. It shows that the path loss increases by $4.7\,\mathrm{dB}$ while doubling the soil moisture. However, at higher frequency of $900\,\mathrm{MHz}$, path loss changes from $138.6\,\mathrm{dB}$ to $131.4\,\mathrm{dB}$ at VWC $40\,\%$ and $20\,\%$, receptively. Hence, the di erence increase to $7.2\,\mathrm{dB}$.

5.3.3 Capacity Analysis

This section analyzes the underground communication on the basis of channel capacity and measure the impact of soil moisture. the parameters of analysis are as follow: transmit power of $10\,\mathrm{dBm}$, noise power density is $1.5625 \times 10^{-16}\,\mathrm{W\,Hz^{-1}}$ [33, 44], maximum bandwidth of the system is same. Although, new specific modulation schemes are needed to use the said maximum bandwidth, however, it is out of the scope of this discussion.

Fig. 5.3(d) plots channel capacity, calculated by equation 5.1, with operational frequency. It shows the optimal frequency for each soil moisture level where the capacity is maximum. The channel capacity ranges from $38\,\mathrm{kbps}$-$70\,\mathrm{kbps}$for VWC ranging from $20\,\%$ - $40\,\%$. As in the case of antenna return loss, the operational frequency decreases with the increase in soil moisture. The interesting thing to note is that the optimal frequency, at which channel capacity is maximum, is much lower than the resonant frequency, e.g., at $20\,\%$ VWC the optimal frequency ($611\,\mathrm{MHz}$) is $38\,\mathrm{MHz}$ lower than the resonant frequency ($649\,\mathrm{MHz}$). This is mainly because though the system bandwidth is highest at resonant frequency but noise power also increases because of noise power density N_0 being a constant. Moreover, as earlier shown in Fig. 5.3(c), path loss decrease with decrease in frequency [37, 40].

Fig. 5.3(e) plots channel capacity with optimal frequency as a function of VWC along with di erent soil types (clay and sandy). It can be observed that soil moisture and optimal frequency are inversely proportional where, for clay soil, a decrease in soil moisture from $40\,\%$ to $10\,\%$ cause optimal operational frequency to increase form $409\,\mathrm{MHz}$ to $833\,\mathrm{MHz}$ and for sandy soil, the optimal frequency is between the range of $393.1\,\mathrm{MHz}$ and $778.6\,\mathrm{MHz}$. It shows that frequency moves in a wide spectrum

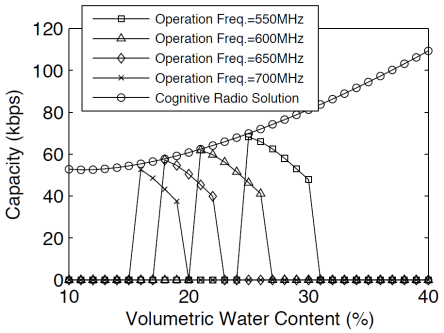

Fig. 5.4: Comparison of channel capacity from non-cognitive (fixed frequency system) and cognitive radio system [10]

with change in soil moisture, therefore, the transceivers employed in WUSNs must be able to operate in wide and lower spectrum range depending on soil moisture values.

Channel capacity shows irregular behaviors in response to change in soil moisture especially in clay soil. For clay soil, there is a slight decrease in channel capacity for VWC increase of $10\,\%$ to $11\,\%$ and then increases to $109.3\,\mathrm{kbps}$ for VWC = $40\,\%$ because of impact of soil moisture and operation frequency on path loss. From Fig. 5.3(c), path loss is inversely proportional to the soil moisture at same operational frequency and increase monotonically with increasing frequency. Even though the path loss increase with soil moisture, it also causes the decrease in optimal operational frequency because of wavelength shortening and low frequency in response to low path loss. Hence, overall path loss of the system may not decrease with the increasing soil moisture. This holds true for the sandy soil as well where capacity is the direct function of soil moisture because sandy soil has relatively lower attenuation from clay soil especially for high soil moisture levels.

Sandy soil has much higher channel capacity then clay soil for all of the soil moisture levels. The channel capacity of sandy soil ($94.22\,\mathrm{kbps}$) is $78.2\,\%$ higher than clay soil ($52.86\,\mathrm{kbps}$) at VWC = $10\,\%$. Similarly, at VWC = $40\,\%$, The channel capacity of sandy soil ($307.8\,\mathrm{kbps}$) is $181.6\,\%$ higher than clay soil ($109.3\,\mathrm{kbps}$). This behavior is due to lower path loss in sandy soil [42]. In practical applications, soil type cannot be changes, however, antenna size can be changed. Fig. 5.3(f) plots operational frequency and corresponding capacity at di erent di erent sized antennas. The lengths of antennas are kept at $60\,\mathrm{mm}$, $100\,\mathrm{mm}$ and $140\,\mathrm{mm}$ in a clay soil. It was observed that as the antenna size increased (longer antenna), the capacity also increased. This is because for longer antennas, the optimal operation frequency also decreased, hence, experiencing low path loss at lower frequency. At VWC = $15\,\%$, the operational frequency and corresponding capacity, in pair, was given as ($703.4\,\mathrm{MHz}$, $54.42\,\mathrm{kbps}$) for $60\,\mathrm{mm}$ antenna, ($443.4\,\mathrm{MHz}$, $455.2\,\mathrm{kbps}$) for $100\,\mathrm{mm}$ antenna, and ($314.6\,\mathrm{MHz}$, $1680\,\mathrm{kbps}$) for $140\,\mathrm{mm}$ antenna. It can be seen that frequency is decreasing and capacity is increasing with increase in antenna size. The di erence becomes greater with increase in soil moisture. For a soil moisture of

VWC = $40\,\%$, the capacity increases from $109.3\,\mathrm{kbps}$ to $3221\,\mathrm{kbps}$ when antenna size increase from $60\,\mathrm{mm}$ to $140\,\mathrm{mm}$. Therefore, the analysis shows that long antennas are suitable for achieving lower path loss. However, the size depends upon the device and availability of the spectrum. It is also hard to employ longer antennas in underground environment [38].

Fig. 5.4 performs the comparison of the fixed frequency systems with cognitive radio system in clay soil. Four fixed frequency systems are operating at $550\,\mathrm{MHz}$, $600\,\mathrm{MHz}$, $650\,\mathrm{MHz}$ and $700\,\mathrm{MHz}$ and cognitive radios dynamically adjust its frequency with the soil moisture levels. For a fixed soil moisture level, the performance of both systems, in terms of channel capacity, is same, e.g., $600\,\mathrm{MHz}$ system has same capacity as of cognitive radio at VWC = $21\,\%$. However, it is not true when the soil moisture level varies, in which case, cognitive radio have better performance as compared to fixed-frequency system. Another important advantage of cognitive radios is that it can sustain capacity higher than the $50\,\mathrm{kbps}$ within wide range of soil moisture level which is not possible with the fixed-frequency systems. For example, with fixed operational frequency of $550\,\mathrm{MHz}$, system is operation with VWC in range of $25\,\%$to $30\,\%$ and this VWC range is $16\,\%$ to $19\,\%$ for fixed operational frequency of $700\,\mathrm{MHz}$ [34, 43].

5.4 Underground Multi-Carrier Capacity

A communication system is evaluated using probability of bit error rate as a metric for SNR values and data rate. However, UG nodes has very low transmission power to achieve a prolonged operating period. Therefore, achievable data rate of wireless underground channel must be estimated for a fixed BER considering the low transmission power of UG nodes. Coherence bandwidth is used as sub-carrier bandwidth for ISI avoidance. It is known that channel capacity changes with the bandwidth [20, 36], hence, it is highly recommended to use bandwidth of sender and receiver antenna pair and channel transfer function of the UG channel while evaluating the capacity of UG channel. Bandwidth of the channel is calculated from the return loss of the antenna. The e ect of soil moisture and soil type on wireless UG channel is studied using multi-carrier modulation. The coherence bandwidth changes are adapted as per soil moisture changes, hence, adapting sub-carrier bandwidth and the system accordingly [39, 44].

The number of sub-carrier in a multi-carrier modulation are minimum number required for inter-symbol interference (ISI) avoidance. If B_s denotes the system bandwidth, B_{cb} denote the UG channel coherence bandwidth, then total number of sub-carriers are given as $N_c = \lceil B_s / B_{cb} \rceil$. B_s is dependent upon the antenna bandwidth. Antenna bandwidth is calculated form its own return loss below a threshold value δ (e.g., [9] uses $\delta = -10\,\mathrm{dB}$).

Fig. 4.2(a) shows the experiment results where return loss of a dipole antenna operating at $433\,\mathrm{MHz}$ and saturated condition, i.e., soil matric potential = 0. Three di erent types of soils are used for this experiment. Bandwidth variation can also be

seen whereas B_{cb} rely on channel characteristics. Empirical coherence bandwidth values are used for the analysis. These values are obtained form time domain impulse response measurements and will be measure in testbed and field experiments [44].

The modulation scheme considered to determine the UG channel capacity is M-ary quadrature amplitude modulation (MQAM). This modulation scheme is used for each carrier of multi-carrier transmission system due to its high spectral efficiency[19]. The total UG channel bit rate is given as $R_{ug} = \sum_{i=1}^{N_c} r_i B_{cb}$, where N_c is the total number of sub carriers, B_{cb} is the the bandwidth of each sub-carrier and r_i represents number of bits per symbol for each carrier [51].

For maximum UG channel bit rate R_{ug}, optimized power allocation can be done between all sub-carriers on the basis of a) fixed power constraint P, and b) probability of symbol error of each sub-carrier, $P_{sc}^* > P_{sc_i}, \forall i$.

The overall bit rate is given as [15]:

$$R_{ug} = \sum_{i=1}^{N_c} B_{cb}\, log_2 \left\{ 1 + \frac{\frac{3\gamma_i P}{(N_0 B_{cb})|H_i(f)|^2}}{\left[Q^{-1}\left\{\frac{P_{sc}^*}{K_{r_i}}\right\}\right]^2} \right\}, \tag{5.3}$$

where P is transmit power constraint, N_c represents the number of sub-carriers, and γ_i's are selected such that $\sum_{i=1}^{N_c} \gamma_i \cdot P = P, \quad \gamma_i > 0$.

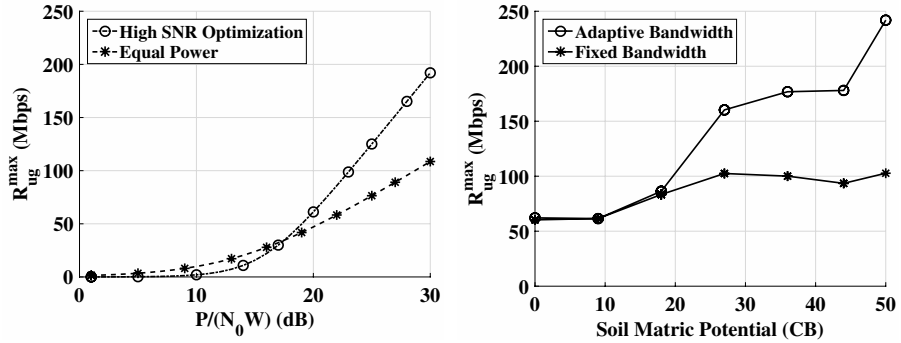

(a) (b)

Fig. 5.5: (a) High-SNR optimization in the silty clay loam soil and (b) System bandwidth approaches

As discussed, the power between each sub-carrier is optimized to achieve maximum R_{ug}. This optimization problem [21], [50] of achieving optimum power allocation γ_i^* can be solved as water filling problem [6], [5] was solved by using a Lagrangian multiplier technique. Fig. 5.5(a) shows the initial comparison of this approach with

that of simple power allocation. This experiment is performed for silty clay loam soil. It can be seen that when equal power distribution is utilized, it results in higher data rate for low $P/(N_0W)$ values of less than $17\,\mathrm{dB}$. Therefore, this technique can be used as default in scenarios with mobile data collection when data collector is moving near the UG radio. The allocation can then be improved according to the improvement in channel state. It will give enough time to gauge the state of UG channel without any performance degradation [47, 49, 52].

Next, multi-carrier modulation capacity is analyzed through detailed antenna return loss and empirical channel transfer function. The experiments are performed in di erent soil types to study the impact of soil types with varying soil moisture levels.

5.4.1 Soil-based UG Channel Estimation

One of the important part of multi-carrier modulation schemes is channel estimation. UG channel is estimated by using two techniques: a) using statistics of soil moisture only, b) extending approach (a) dynamic channel sensing. For first approach uses this channel transfer function to create a configuration database of channel states and impulse responses. The soil moisture measurements are taken at di erent instants and a channel state is selected based on those measurements. Next, a comparative analysis between theoretical (from (5.3)) and experimental multi-carrier communication results for validation.

Second approach an improvement of first one and gives more accurate channel state. It incorporates real-time channel sensing by adding extra hardware for dynamic channel estimation. However, it will also add an extra overhead. UG devices are being improved using advanced technologies making the dynamic channel sensing a feasible solution for UG communication systems [46, 54]. The channel state is not expected to change within close vicinity of a measured soil moisture level area. Hence, a powerful UG node can be used as a master node to perform dynamic channel estimation. This master node can disseminate the channel state to other low power UG nodes. Moreover, dynamic channel sensing is expected to consume more power. Unlike traditional sensing nodes and handheld devices, UG nodes do not have tight size limitations because they are buried. Hence, power consumption problem can be minimized by burying large batteries with UG nodes for prolonged operation.

5.4.2 Adaptive Subcarrier and System Bandwidth

The initial results shows that capacity of UG channel with multi-carrier modulation is e ected by the soil moisture, soil type, and distance between the transmitter and receiver. Similarly, transmission parameters (e.g., sub-carrier bandwidth) can be adjusted to improve performance.

Given these findings, e ect of adaptive sub-carrier bandwidth (ASB) on UG channel capacity was analyzed. In [4, 25], improvements were reported with the use of adaptive channel width, and [7], [45] reported improvements with adaptive sub-carrier bandwidth (ASB). As an initial work, a comparative analyses was performed between theoretical data rate of a fixed sub-carrier ($411\,\mathrm{kHz}$) and system bandwidth ($20\,\mathrm{MHz}$) with an adaptive sub-carrier and system bandwidth approach. Fig. 5.5(b) shows th results for di erent soil moisture levels. For a soil moisture level of 27 CB, fixed approach gives the channel capacity of 102 Mbps and adaptive gives 159 Mbps, i.e., approx. $56\,\%$ higher channel capacity. Similar trend is experienced when the soil moisture is increased to 50 CB with adaptive approach achieving the channel capacity of 241 Mbps, i.e., approx. $136\,\%$ higher than fixed approach.

5.5 Magnetic Induction-Based Wireless Channel Capacity

EM waves can only be used for small communication ranges in underground environment because it su ers from severe impairments due to rocks, soil and sand. Therefore, a feasible alternative is to use Magnetic Induction for underground communication. First MI-based WUSN was used by [2]. In MI-based WUSNs, magnetic coils are used as communication antenna combined using a waveguide structure. Many relay nodes are used between the end nodes to facilitate the communication between two ends [47]. MI-based WUSN, similar to conventional wireless network, takes the advantage of lower pathloss extending the transmission range as compared to its EM-based counterpart. Another advantage of MI-based relaying nodes do not needs to be charged, however, end tranciever nodes needs energy and can be charged using mobile above-ground devices [16]. WUSNs are not demanding in terms of data rate, however, channel characterization of MI-based is important so that it can provide at-least sufficient performance. In this section, a specific MI-based channel modeling scheme is discussed in detail.

5.5.1 System Model

Topology used to model system includes a one sender, one receiver and $k-1$ passive relays. All nodes are connected in a waveguide structure. the voltage source of sender is U_t and load impedance of receiver is Z_l. Relaying nodes are placed equidistantly between both end nodes [47]. Each node circuit consist of an antenna (magnetic), a capacitor C, and a resistor R. The parasitic e ect of a circuit, due to high frequencies is ignored. To that end, such frequency ranges are adopted for which the e ect is negligible. Multilayer air core coil is used as an antenna. The inductivity L and copper resistance R of such antenna coil is given as [2]:

$$L = \frac{21\mu N^2 a}{4\pi}\left(\frac{a}{l+h}\right)^{0.5}, \tag{5.4}$$

$$R = \rho \cdot \frac{l_w}{A_w} = \rho \cdot \frac{2aN}{r_w^2}, \tag{5.5}$$

where N denotes the total coil windings, radius of the coil is a, length of the coil is l = $0.5a$, h and μ denotes the height and permeability of the coil. The capacitance $C = \frac{1}{(2\pi f_0)^2 L}$ is chosen such that the circuit operates at resonant frequency f_0. Moreover, in equation 5.5, $\rho \approx 1.678 \times 10^{-2}\ mm^2/m$ and represents the copper resistivity, l_w, A_w and r_W are the total length, cross-section area and radius of the wire, respectively.The induced voltage is calculated through mutual inductance M [48] as follow:

$$M = \mu\pi N^2 \frac{a^4}{4r^3}(2\sin\theta_t \sin\theta_r + \cos\theta_t \cos\theta_r) \cdot G, \tag{5.6}$$

where θ_t is the angle between radial direction of the coil θ_r is the angle between the line connecting the center of two coils, r gives distance between two coils. An additional loss factor which occurs due to eddy currents is given by G.

Loss in Soil: Magnetic waves su er from extra attenuation due to eddy current [18]. This e ect is considered in this model by using a scaling factor $G = e^{-r/\delta}$ where attenuation factor δ is given as:

$$\delta = \frac{1}{2\pi f\sqrt{\frac{\mu\epsilon}{2}\left(\sqrt{1+\frac{\sigma^2}{(2\pi f)^2\epsilon^2}}-1\right)}}, \tag{5.7}$$

where ϵ is permittivity and σ is conductivity of the soil, f is the frequency.

Path Loss: The path loss the system is calculated as [17]:

$$L_p(f) = \left|\frac{P_t(f)}{P_r(f)}\right| = \frac{|S(x,x_L,k)\cdot S(x,x_L,k+1)|}{|\text{Im}\{x_L\}|}, \tag{5.8}$$

where $P_t(f)$ is the required transmit power given as:

$$P_t(f) = \frac{1}{2}|U_t \cdot I_0| = \frac{1}{2}\frac{|U_t|^2}{|j2\pi f M|}\frac{|S(x,x_L,k)|}{|S(x,x_L,k+1)|} \tag{5.9}$$

and $P_r(f)$ is the active received power given as:

$$P_r(f) = \frac{1}{2}|I_k|^2 \text{Re}\{Z_L\} = \frac{|U_t|^2 \cdot \text{Re}\{Z_L\}}{2|j2\pi f M|^2 |S(x,x_L,k+1)|^2} \tag{5.10}$$

where the induced voltage of coil $n-1$ is $U_n = j2\pi f M$ and

$$S(x, x_L, n) = F(x, n) + x_L \cdot F(x, n-1),$$
$$F(x,n) = \frac{\left(\frac{(x+\sqrt{x^2-4})}{2}\right)^{n+1} - \left(\frac{(x-\sqrt{x^2-4})}{2}\right)^{n+1}}{\sqrt{x^2-4}}$$

Load Impedance: The element of the circuits are susceptible to noise and can degrade the performance of the system, hence, the simplest possible load impedance is given as [17]:

$$Z_L = Z_{L,R} = \text{Re}\left\{ j2\pi f_0 M \cdot \frac{F(x_0,k+1)}{F(x_0,k)} \right\} \tag{5.11}$$

where $x_0 = \frac{R}{j2\pi f_0 JM}$ because of the very limited bandwidth of MI-based systems [47].

Noise Modeling Although there can be many random noise sources in the environment. The noise is basically EM waves $10\,\text{cm}$ and given the high EM attenuation in the soil, the e ect of these waves can be minimized to a large extent. Therefore, only thermal noise, from resistors of relay and end nodes, is considered as a dominant source. Noise power at load impedance is given as [17]:

$$P_{N,R}(f) = \frac{1}{2}\frac{Z_{L,R}}{|j2\pi fM|^2} \times \left| \sum_{m=0}^{k} \left(\sum_{n=0}^{m} U_{R,k-n} \frac{S(x,x_L,n)}{S(x,x_L,m)S(x,x_L,m+1)} \right) \right|^2 \tag{5.12}$$

If all the noise sources are independent with Johnson-noise [12] power spectral densities $\text{E}\{|U_{R,n}(f)|^2\} = 4KTR,\ \forall\, n$ ($\text{E}\{\cdot\}$ = expected value), then average noise power due to resistor is given as:

$$\text{E}\{P_{N,R}(f)\} = \frac{1}{2}\frac{4KTRZ_{L,R}}{|j2\pi fM|^2}$$
$$\times \sum_{n=0}^{k} \left(|S(x,x_L,n)|^2 \left| \sum_{m=n}^{k} \frac{1}{S(x,x_L,m)S(x,x_L,m+1)} \right|^2 \right).$$

where Boltzmann constant $K \approx 1.38 \times 10^{-23}$ J/K, temperature in Kelvin is $T = 290K$ and R is the copper resistance from equation 5.2.
Similarly, noise from the resistor with power density $\text{E}\{|U_{Z_{L,R}}(f)|^2\} = 4KTZ_{L,R}$ is given as:

$$\mathrm{E}\{P_{N,Z_{LR}}(f)\} = \frac{1}{2}\frac{4KTZ_{L,R}^2}{|j2\pi fM|^2} \times \left|\sum_{m=0}^{k}\frac{1}{S(x,x_L,m)S(x,x_L,m+1)}\right|^2.$$

Finally, total power spectral density of noise for load resistor is given as:

$$\mathrm{E}\{P_{\text{noise}}(f)\} = \mathrm{E}\{P_{N,R}(f)\} + \mathrm{E}\{P_{N},Z_{L,R}(f)\}. \tag{5.13}$$

5.5.2 Channel Capacity

To maximize the channel capacity of the system it is important to find the optimal waveguide parameters. To that end, three paramters are chosen: the number of coil windings, transmit power density spectrum, and the carrier frequency. Other parameters are either not possible to change or dependent upon these parameters. The optimization problem is given as follow [17] :

$$\begin{aligned}\underset{\forall f_0,N,P_t(f)}{\arg\max}\ C_{ch} &= \int_{-\infty}^{+\infty}\log_2\left(1+\frac{P_t(f)}{L_p(f)\mathrm{E}\{P_{\text{noise}}(f)\}}\right)\mathrm{d}f \\ \text{s.t.}: \quad (1)&\int_{-\infty}^{+\infty}P_t(f)\mathrm{d}f = P, \qquad (2)N\in[N_{\min},N_{\max}], \\ (3)&f_0\in[f_{0,\min},f_{0,\max}], \quad (4)\frac{1}{(2\pi f_0)^2L}\geq C_0,\end{aligned} \tag{5.14}$$

where channel capacity is given as C_{ch} [17], and total power transmitted is P. The transmit power spectral density is denoted by $P_t(f)$. $P_t(f)$ can be adjusted by $U_t.L_p(f)$ (from equation 5.8) and $\mathrm{E}\{P_{noise}(f)\}$ (from equation 5.11). Some of the limitations, imposed on the systems, are: (1) limited number of coil windings are used in the range of $[N_{min}, N_{max}]$ as size of the relay nodes can cause an issue while deployment, (2) lower frequency ranges ($f_{0,min}$ =1 kHz, $f_{0,max}$ =300 MHz) are used to avoid parasitic e ect. However, higher carrier frequencies with larger number of windings results in the low capacitance increasing the parasitic resistance significantly [46]. Hence, a lower bound on the the penitence C_0 is applied.

Optimization Algorithm for Channel Capacity A 2-dimensional grid is spanned over extreme values of f_0 and N. Capacity is determined for each grid point over multiple iterations X_I. The grid point having the largest capacity is selected as a region of interest for each iteration of the algorithm. The values of f_0 and N are selected as per the constraints given equation 5.14. A total of 40 grid points are used for the f_0 and 10 for N. The f_0 points are exponentially separated instead of being equidistant because of large di erence in minimum and maximum values of f_0. Moreover, if a point is not in accordance with the

constraint 4 of equation 5.14, channel capacity is set to zero. For other points, an optimal transmit power spectral density $P_t(f)$ is evaluated using water filling [49] as follow:

$$P_t(f) = \max\left(\left(\frac{1}{\lambda} - L_p(f)\mathrm{E}\{P_{\text{noise}}(f)\}\right), 0\right), \tag{5.15}$$

where λ is adapts to satisfy the constraint 4. The equation 5.15 is integrated in equation 5.14 which gives the channel capacity for a particular (f_0,N).

5.5.3 Numerical Results

Table 5.1: Parameters

Parameters	Description	Values
P	Total Transmit Power	$10\,\mathrm{mW}$
r_w	Wire Radius	$0.5\,\mathrm{mm}$
a	Coil Radius	4
σ	Coil Conductivity	$0.01\,\mathrm{S/m}$ for dry soil; $0.077\,\mathrm{S/m}$ for wet soil
ϵ_0	Electric constant	$8.854 \times 10^{-12}\,\mathrm{F/m}$
ϵ	Soil Permittivity	$\epsilon = 7\epsilon_0$ for dry soil; $\epsilon = 29\epsilon_0$ for wet soil
$\mu_0 = \mu$	Magnetic constant	$4\pi{\cdot}10^{-7}\ \mathrm{H/m}$

The system is simulated for di erent arrangements of waveguide. Simulation parameters are given in Table 5.1. two di erent deployment schemes, horizontal and vertical, were analyzed [10]. For vertical deployment, θ_t and θ_r were kept equal whereas for horizontal deployment $\theta_t = \pi/2$ and $\theta_r = -\pi/2$ were used. vertical deployment gives the omnidirectional communication range, however, do not maximize the mutual inductance, hence, exhibiting a very high path loss for vertical deployment as given in the following equation.

$$L_{p,\text{vertical}}(f) \approx 2^{2k} \cdot L_{p,\text{horizontal}}(f) \tag{5.16}$$

In Fig. 5.6(a), channel capacity is plotted with t eh carrier frequency with N=1000, 15 relays and total distance of 50m in a dry soil. the constrained capacitance is

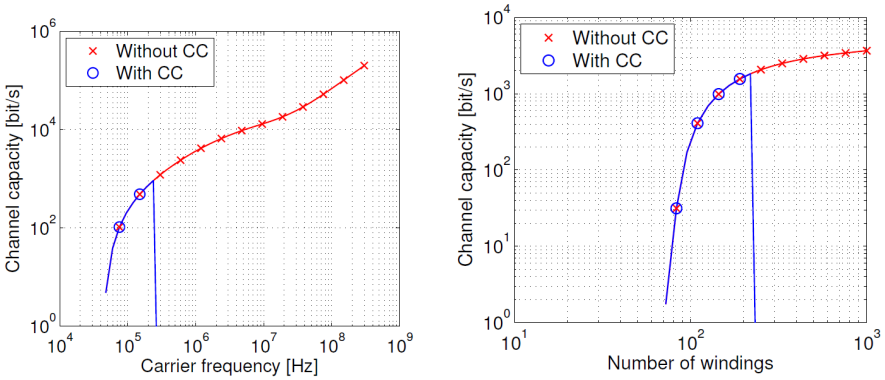

Fig. 5.6: (a) E ect of carrier frequency on Channel capacity [17]; (b) E ect of number of windings on Channel capacity at constant frequency [17]

$C_0 = 1pf$. Fig. 5.6(a) shows the results for both constrained and unconstrained capacitance. Low capacity is observed for the constrained channel capacitance and, for unconstrained capacitance, channel capacity is high at large values of the frequency. Similar kind of behavior is observed in Fig. 5.6(b) where capacity is plotted with total number of windings at a constant frequency of $f_0 = 1\,\text{MHz}$. Capacity is low for the constrained scenario and high for unconstrained scenario. Hence, both f_0 and N needs to be optimized together.

Fig. 5.7 give the capacity results for optimum values of N and f_0. It plots the optimum capacity with minimum capacitance C_0 for $X_I = 4$ iterations. For large values of C_0, the channel capacity decreases more in dry soil than wet soil. Capacitor constraints do not e ect the performance in wet soil because the constrain do not let maximum carrier frequency go significant lower than optimal carrier frequency.

Fig. 5.8 plots the channel capacity with the inter-relay distance. Parameters for the experiments are as follow: $C_0 = 1$pF, $B = 100\,\text{MHz}$, and $f_0 = 300\,\text{MHz}$. It is also compared with EM-based communication where noise power of EM-based transmission is $P_{noise,EM} = KTB$ [16]. Four di erent constellations were used for the MI-based communication: Direct MI (written as only MI in the figure), MI-waveguides for distances of 3, 4, and 5 meters represented by MI-WG-3m, MI-WG-4m, and MI-WG-5m, respectively, in the Fig. 5.8. Here, minimum distance refer to highest number of relay nodes. It was observed that EM-based transmission is e ective for only $d < 7$ in dry soil. For wet soil, EM-based communication performance is always less than the MI-based. Under constrained capacitance the performance of the MI-waveguides su ers badly even less than the direct MI in case of 4 m and 5 m. MI-waveguides with 3m intercoil distance are performing well for the $d > 45$m. Although, MI-waveguide with high relay density, i.e., 3 m intercoil

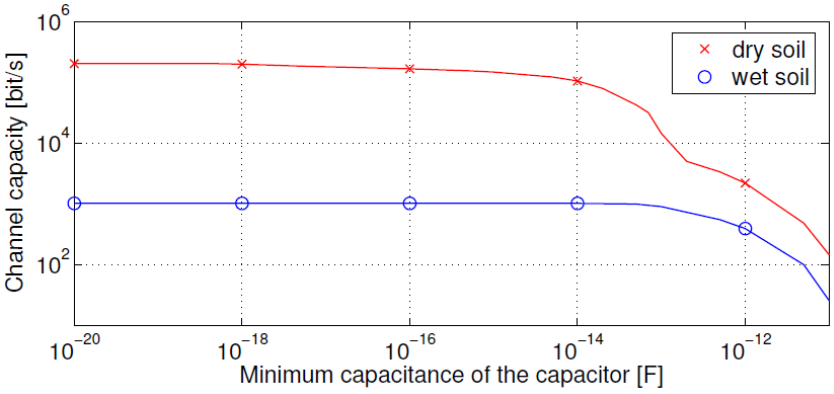

Fig. 5.7: E ect of capacitance on channel capacity [17]

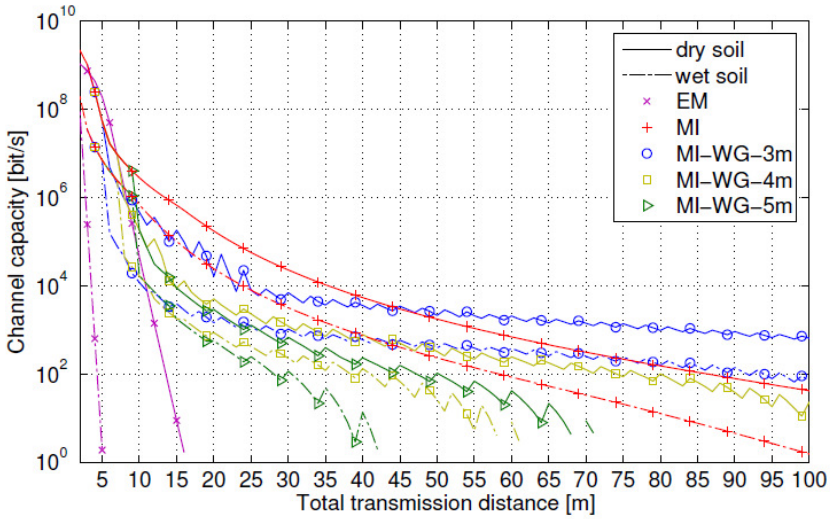

Fig. 5.8: Channel capacity for EM-based and di erent MI-based WUCs [17]

distance, increases the channel capacity (600 bits/s) and communication distance (100m), however, deployment e ort (deploying nodes and adjusting their angles) should also be considered for this case. Therefore, it is a trade-o between the relay efficiency and deployment e ort.

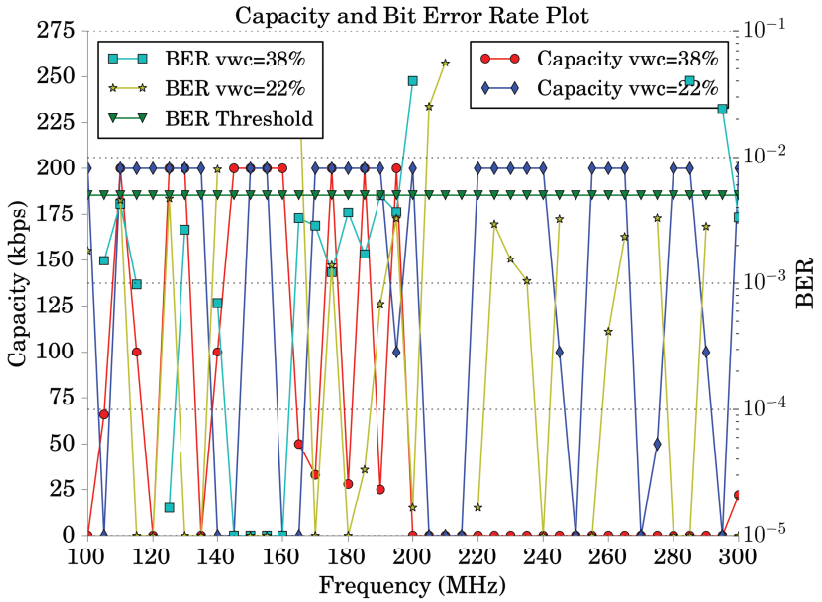

Fig. 5.9: Capacity and BER Plot - 200k - Di erent Soil Moisture Values

5.6 Bit Error Rate (BER) Analysis

Experimental analysis of the BER in wireless underground channel is challenging due to the factors. First, when an electromagnetic wave is incident into soil, the wavelength changes because of the higher permittivity of soil compared to that of air. Soil permittivity depends on soil properties, such as bulk density, soil texture, soil moisture (volumetric water content),salinity, and temperature. Second, when an antenna is buried underground, its return loss property changes due to the high permittivity of the soil. Moreover, with the variation in soil moisture and, hence, soil permittivity, the return loss of the antenna varies too.

The BER statistics performance of channel are used to design error control schemes. For these experiments, the error statistics from [14] and [43] are used. These statistics are important to ascertain the channel behavior under di erent condition and are useful in designing error coding schemes. A relation between BER and channel capacity has been established that can obtain capacity of channel in terms of BER obtained by experiments without knowledge of statistical characterizations (such as PDF, cumulative distribution function (CDF), moment generating function (MGF), moments, Laguerre moments, etc.).

Following bit error statistics are implemented:

- Bit error rate

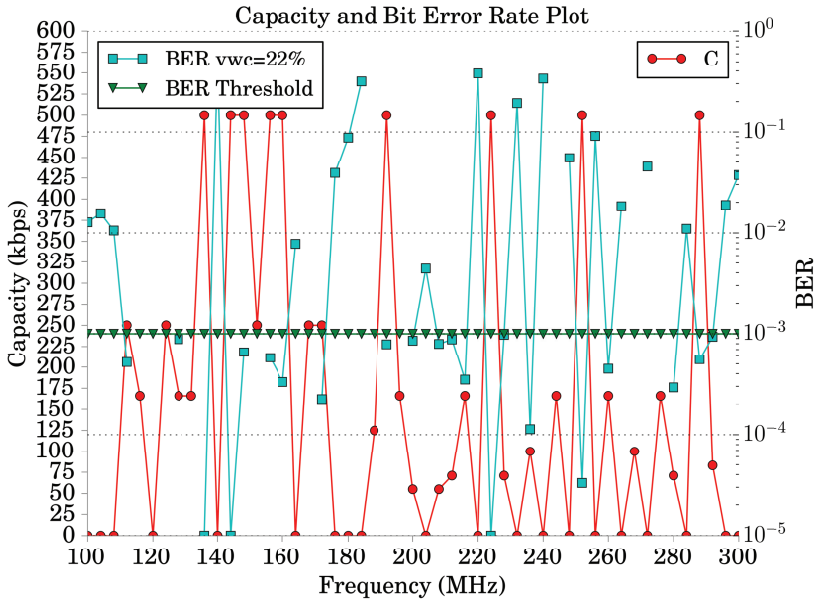

Fig. 5.10: Capacity and BER Plot - 500k

- Probability of burst of length b, P(b)
- Burst count of each burst length n
- O set to start symbol
- Positions of bits in error of all symbol
- Number of correctly received symbols
- No of bits in error per symbol
- Average no of bits in error

The experiments are conducted for frequency range of $100\,\mathrm{MHz}$ to $600\,\mathrm{MHz}$ using GNU Radio [10] and USRPs [9]. The 500K and 200K channel bandwidth are employed for these experiments.The dipole antennas are used in these experiments. A series of sequences of 1000 bits long are sent from transmitter and at the receiver side error statistics of the channel are obtained by comparing the output with input. For each frequency,the bit error rate is calculated by adding the bits in error of each correct symbol and then dividing this sum by total number of bits in all correctly decoded symbols.

Fig. 5.9 is of two experiments with volumetric water content $38\,\%$ and $22\,\%$ respectively. These experimental results verifies two theoretical capacity analysis findings and the strengthen the cognitive radio argument that to achieve capacity the transmitters receivers in underground channel should be able to work in wide range of spectrum:

First, Fig. 5.9 shows that with increase in soil moisture (VWC 38 %) optimal frequency is between 100 MHz to 200 MHz and with decrease in soil moisture (VWC = 22 %) optimal frequency is between 100 MHz to 300 MHz. As the soil moisture increases, the optimal operation frequency shifts to the lower spectrum. It also verifies that optimal operation frequency is a monotonically decreasing function of soil moisture.

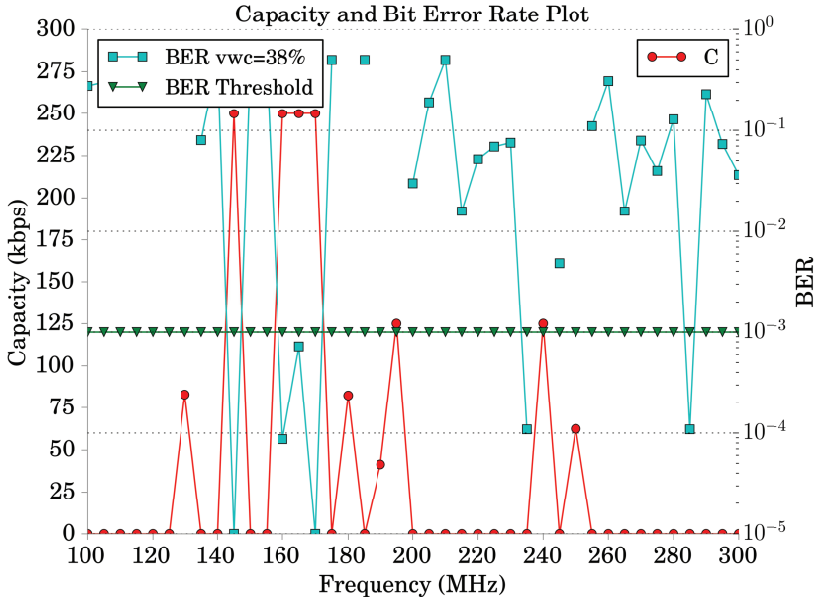

Fig. 5.11: Capacity and BER Plot - 250k

Second we can also see that for between 200 MHz to 300 MHz, for a fixed frequency capacity decreases with increase in soil moisture.

Third, for the the lower spectrum i.e operation frequency less than 200 MHz, channel capacity does not change with increase in soil moisture for most of frequencies whereas for some frequencies it is less than capacity of low soil moisture case.

Analysis of these plots reveals that higher bandwidth su ers more attenuation in soil and hence results in higher error rates. In 500K experiments for all four depths, bit error rates are very high.For frequencies where symbols were decoded correctly, bit error rate is around 10^{-1} the 10^{-2} (shown by red dots on the graph), for rest of the frequencies where symbols were decoded in error are shown as 10^{0}.

Second, increasing depth also increases error rate. For example, for 10 cm depth we decodes symbols in more wider span of frequencies as compared to 40 cm depth where we decoded symbols only in fewer frequencies range. For 10 Cm depth fewer

symbols were in error than 40 cm depth. Going deep from 10 cm to 40 cm also decreases correctly received bits at higher frequencies.

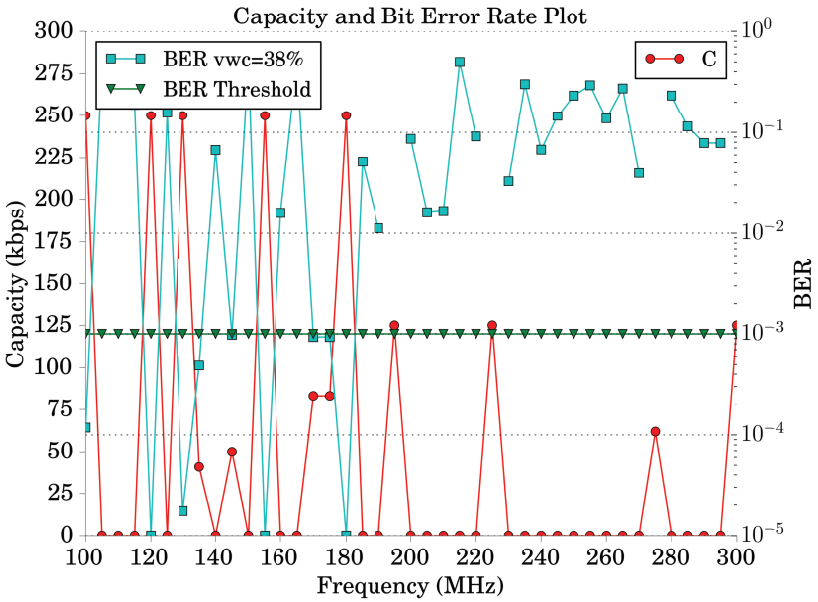

Fig. 5.12: Capacity and BER plot for 250k bandwidth.

Here in frequency range of 150 MHz to 190 MHz error rate is less than 10^{-3}. Frequency range of symbols decoded with less errors is aligned with antenna return loss 120 MHz to 230 MHz, and 490 MHz to 540 MHz. This underscores the importance of lower bandwidths and wideband planner antennas in wireless underground sensor networks.

Fig. 5.10 shows the capacity for 500k rate experiments. It shows that capacity for the range of 200 MHz to 300 MHz the is less than 200k case this is because of low BER threshold used to analyses 500k experiment. It also shows that rate for 140 MHz to 160 MHz is higher in 500k experiment as compared to 200k case.

Fig. 5.11 and Fig. 5.12 shows the rate for two 250k rate experiments for VWC value of 38 %. This matches with the results of 200k experiments.

5.7 Open Research Issues

The BER analysis investigations confirms that lower frequencies are more suitable for Wireless Underground Sensor Networks (WUSNs) communication, as higher

frequencies exhibits more error rate as compared to lower spectrum. Our BER results also underground channel capacity may be limited up-to few hundred kilobits per second. Our initial findings also show that higher soil moisture also e ects underground channel communications.

For future work, we plan to conduct more experiments to continue validating theoretical model with channel sounding and multi-paths experiments. We also plan to use lower rate and bandwidth to ascertain channel capacity [41, 51]. Our findings also show that antenna return loss also e ects underground channel communications. We plan to conduct these experiments with planner antennas. We also plan characterize e ects of soil moisture, soil properties, and antennas by developing a highly robust, flexible and configurable testbed in which these parameters, i.e soil layers, soil moisture etc can be controlled efficiently and expediently [49, 52].

References

[2] Akyildiz IF, Stuntebeck EP (2006) Wireless underground sensor networks: Research challenges. Ad Hoc Networks 4(6):669–686

[2] Beckmann HW, Lampe K, Milde H, Rohlfing H, Scheurmann M, Tornau F, Zantis F (1998) Friedrich tabellenbuch elektrotechnik/elektronik

[9] Bird TS (2009) Definition and misuse of return loss [Report of the transactions Editor-in-Chief]. IEEE Antennas and Propagation Magazine 51(2):166–167, DOI 10.1109/MAP.2009.5162049

[4] Chandra R, Mahajan R, Moscibroda T, Raghavendra R, Bahl P (2008) A case for adapting channel width in wireless networks. SIGCOMM Comput Commun Rev 38(4):135–146, DOI 10.1145/1402946.1402975, URL `http://doi.acm.org/10.1145/1402946.1402975`

[5] Cheng R, Verdu S (1993) Gaussian multiaccess channels with ISI: capacity region and multiuser water-filling. IEEE Trans Information Theory 39(3):773–785, DOI 10.1109/18.256487

[6] Cover TM, Thomas JA (2006) Elements of Information Theory 2nd Edition. Wiley-Interscience

[7] Das S, de Carvalho E, Prasad R (2008) Performance analysis of OFDM systems with adaptive sub carrier bandwidth. IEEE Trans Wireless Communications 7(4):1117–1122, DOI 10.1109/TWC.2008.060761

[8] Dong X, Vuran MC (2020) Return loss analysis of antennas in wireless underground sensor networks, submitted

[61] Dong X, Vuran MC (2011) A channel model for wireless underground sensor networks using lateral waves. In: Proc. of IEEE Globecom '11, Houston, TX

[10] Dong X, Vuran MC (2013) Impacts of soil moisture on cognitive radio underground networks. In: 2013 First International Black Sea Conference on Communications and Networking (BlackSeaCom), IEEE, pp 222–227

[9] Ettus Research Website (2016) URL `http://www.ettus.com`

[12] Friis HT (1944) Noise figures of radio receivers. Proceedings of the IRE 32(7):419–422
[10] GNU Radio Website (2020) URL http://www.gnuradio.org
[14] Jagath-Kumara KDR, Bebbington M (2005) Error content in frames transmitted over burst-error channels. Wireless Communications, IEEE Transactions on 4(5):2533–2539
[15] Kalet I (1989) The multitone channel. IEEE Trans Communications 37(2):119–124, DOI 10.1109/26.20079
[16] Karalis A, Joannopoulos JD, Soljačić M (2008) Efficient wireless non-radiative mid-range energy transfer. Annals of physics 323(1):34–48
[17] Kissele S, Gerstacker W, Schober R, Sun Z, Akyildiz IF (2013) Channel capacity of magnetic induction based wireless underground sensor networks under practical constraints. In: 2013 IEEE Wireless Communications and Networking Conference (WCNC), IEEE, pp 2603–2608
[18] Kriezis E, Tsiboukis TD, Panas SM, Tegopoulos JA (1992) Eddy currents: Theory and applications. Proceedings of the IEEE 80(10):1559–1589
[19] Ma R, Zhang W (2015) Adaptive MQAM for energy harvesting wireless communications with 1-bit channel feedback. IEEE Trans Wireless Communications PP(99):1–1, DOI 10.1109/TWC.2015.2455494
[20] Proakis J, Salehi M (2007) Digital Communications, 5th edn. McGraw-Hill
[21] Rhee W, Cioffi J (2000) Increase in capacity of multiuser ofdm system using dynamic subchannel allocation. In: Proc. IEEE 51st VTC 2000-Spring, Tokyo, Japan, DOI 10.1109/VETECS.2000.851292
[25] Salam A (2019) A comparison of path loss variations in soil using planar and dipole antennas. In: 2019 IEEE International Symposium on Antennas and Propagation, IEEE
[26] Salam A (2019) Design of subsurface phased array antennas for digital agriculture applications. In: Proc. 2019 IEEE International Symposium on Phased Array Systems and Technology (IEEE Array 2019), Waltham, MA, USA
[29] Salam A (2019) Subsurface mimo: A beamforming design in internet of underground things for digital agriculture applications. Journal of Sensor and Actuator Networks 8(3), DOI 10.3390/jsan8030041, URL https://www.mdpi.com/2224-2708/8/3/41
[33] Salam A (2020) Internet of Things for Environmental Sustainability and Climate Change, Springer International Publishing, Cham, pp 33–69. DOI 10.1007/978-3-030-35291-2_2, URL https://doi.org/10.1007/978-3-030-35291-2_2
[34] Salam A (2020) Internet of Things for Sustainability: Perspectives in Privacy, Cybersecurity, and Future Trends, Springer International Publishing, Cham, pp 299–327. DOI 10.1007/978-3-030-35291-2_10, URL https://doi.org/10.1007/978-3-030-35291-2_10
[35] Salam A (2020) Internet of Things for Sustainable Community Development, 1st edn. Springer Nature, DOI 10.1007/978-3-030-35291-2
[36] Salam A (2020) Internet of Things for Sustainable Community Development: Introduction and Overview, Springer International Publishing, Cham, pp 1–31.

DOI 10.1007/978-3-030-35291-2_1, URL https://doi.org/10.1007/978-3-030-35291-2_1

[37] Salam A (2020) Internet of Things for Sustainable Forestry, Springer International Publishing, Cham, pp 147–181. DOI 10.1007/978-3-030-35291-2_5, URL https://doi.org/10.1007/978-3-030-35291-2_5

[38] Salam A (2020) Internet of Things for Sustainable Human Health, Springer International Publishing, Cham, pp 217–242. DOI 10.1007/978-3-030-35291-2_7, URL https://doi.org/10.1007/978-3-030-35291-2_7

[39] Salam A (2020) Internet of Things for Sustainable Mining, Springer International Publishing, Cham, pp 243–271. DOI 10.1007/978-3-030-35291-2_8, URL https://doi.org/10.1007/978-3-030-35291-2_8

[40] Salam A (2020) Internet of Things for Water Sustainability, Springer International Publishing, Cham, pp 113–145. DOI 10.1007/978-3-030-35291-2_4, URL https://doi.org/10.1007/978-3-030-35291-2_4

[41] Salam A (2020) Internet of Things in Agricultural Innovation and Security, Springer International Publishing, Cham, pp 71–112. DOI 10.1007/978-3-030-35291-2_3, URL https://doi.org/10.1007/978-3-030-35291-2_3

[42] Salam A (2020) Internet of Things in Sustainable Energy Systems, Springer International Publishing, Cham, pp 183–216. DOI 10.1007/978-3-030-35291-2_6, URL https://doi.org/10.1007/978-3-030-35291-2_6

[43] Salam A (2020) Internet of Things in Water Management and Treatment, Springer International Publishing, Cham, pp 273–298. DOI 10.1007/978-3-030-35291-2_9, URL https://doi.org/10.1007/978-3-030-35291-2_9

[44] Salam A (2020) Wireless underground communications in sewer and stormwater overflow monitoring: Radio waves through soil and asphalt medium. Information 11(2)

[46] Salam A, Shah S (2019) Internet of things in smart agriculture: Enabling technologies. In: 2019 IEEE 5th World Forum on Internet of Things (WF-IoT), IEEE, pp 692–695

[47] Salam A, Vuran MC (2016) Impacts of soil type and moisture on the capacity of multi-carrier modulation in internet of underground things. In: Proc. of the 25th ICCCN 2016, Waikoloa, Hawaii, USA

[49] Salam A, Vuran MC (2017) Smart underground antenna arrays: A soil moisture adaptive beamforming approach. In: Proc. IEEE INFOCOM 2017, Atlanta, USA

[51] Salam A, Vuran MC, Irmak S (2016) Pulses in the sand: Impulse response analysis of wireless underground channel. In: The 35th Annual IEEE International Conference on Computer Communications (INFOCOM 2016), San Francisco, USA

[52] Salam A, Vuran MC, Irmak S (2017) Towards internet of underground things in smart lighting: A statistical model of wireless underground channel. In: Proc. 14th IEEE International Conference on Networking, Sensing and Control (IEEE ICNSC), Calabria, Italy

[54] Salam A, Vuran MC, Dong X, Argyropoulos C, Irmak S (2019) A theoretical model of underground dipole antennas for communications in internet of underground things. IEEE Transactions on Antennas and Propagation

[43] Salih O, Wang C, Ai B, Mesleh R (2014) Adaptive generative models for digital wireless channels. Wireless Communications, IEEE Transactions on PP(99):1–1, DOI 10.1109/TWC.2014.2325028

[44] Silva AR, Vuran MC (2009) Empirical evaluation of wireless underground-to-underground communication in wireless underground sensor networks. In: International Conference on Distributed Computing in Sensor Systems, Springer, pp 231–244

[45] Singh S, Shahbazi M, Pelechrinis K, Sundaresan K, Krishnamurthy S, Addepalli S (2015) Adaptive sub-carrier level power allocation in OFDMA networks. IEEE Trans Mobile Computing 14(1):28–41, DOI 10.1109/TMC.2014.2312716

[46] Spyker RL, Nelms RM (2000) Classical equivalent circuit parameters for a double-layer capacitor. IEEE transactions on aerospace and electronic systems 36(3):829–836

[47] Sun Z, Akyildiz I (2010) Magnetic induction communications for wireless underground sensor networks. IEEE Transactions on Antennas and Propagation 58(7):2426 –2435, DOI 10.1109/TAP.2010.2048858

[48] Sun Z, Akyildiz IF (2012) On capacity of magnetic induction-based wireless underground sensor networks. In: 2012 Proceedings IEEE INFOCOM, IEEE, pp 370–378

[49] Tse D, Viswanath P (2005) Fundamentals of wireless communication. Cambridge university press

[50] Xhafa A, Tonguz O, Cepni A, Stancil D, Nikitin P, Brodtkorb D (2005) On the capacity limits of HVAC duct channel for high-speed internet access. IEEE Trans Communications 53(2):335–342, DOI 10.1109/TCOMM.2004.841949